Geophysical Research Letters

RESEARCH LETTER
10.1029/2021GL093416

Fluvial Organic Carbon Composition Regulated by Seasonal Variability in Lowland River Migration and Water Discharge

Nina Y. Golombek[1,2,3], Joel S. Scheingross[1,4], Marisa N. Repasch[1,5], Niels Hovius[1,2], Johanna Menges[1,6], Dirk Sachse[1], Maarten Lupker[7], Timothy I. Eglinton[7], Negar Haghipour[7,8], Simon R. Poulson[4], Darren R. Gröcke[9], Francisco G. Latosinski[10,11], and Ricardo N. Szupiany[10,11]

[1]GFZ—German Research Centre for Geosciences, Potsdam, Germany, [2]Department of Geosciences, University of Potsdam, Potsdam, Germany, [3]Department of Earth and Environmental Sciences, Dalhousie University, Halifax, NS, Canada, [4]Department of Geological Sciences and Engineering, University of Nevada, Reno, NV, USA, [5]Lawrence Livermore National Lab, Livermore, CA, USA, [6]MARUM—Center for Marine Environmental Sciences, University of Bremen, Bremen, Germany, [7]Geological Institute, ETH Zürich, Zürich, Switzerland, [8]Laboratory of Ion Beam Physics, ETH Zürich, Zürich, Switzerland, [9]Department of Earth Sciences, Durham University, Durham, UK, [10]National Council for Scientific and Technological Research (CONICET), Buenos Aires, Argentina, [11]School of Engineering and Water Sciences, Universidad Nacional del Litoral Santa Fe, Santa Fe, Argentina

Abstract Identifying drivers of seasonal variations in fluvial particulate organic carbon (POC) composition can aid sediment provenance and biogeochemical cycling studies. We evaluate seasonal changes in POC composition in the Río Bermejo, Argentina, a lowland river running ~1,270 km without tributaries. Weekly POC concentration and isotopic composition from 2016 to 2018 show that during the wet season, increased lateral channel migration generates an influx of ^{13}C-enriched and ^{14}C-enriched floodplain-sourced material, overprinting the ^{13}C-depleted and ^{14}C-depleted headwater signature that is observed during the dry season. These findings demonstrate how channel morphodynamics can drive variability of POC composition in lowland rivers, and may modulate the composition of POC preserved in sedimentary archives.

Plain Language Summary Reconstruction of past climate conditions is often based on the chemistry of organic matter transported from rivers into ocean basins. However, it is unclear how organic matter chemistry changes from its original continental source to its final sink in ocean basins. As organic matter moves downstream through lowland rivers, this material can be deposited in floodplains. During floodplain storage, organic matter is decomposed and replaced, changing its chemistry and, ultimately the record of past climate. To understand how organic matter chemistry changes seasonally, we collected weekly samples of suspended sediment in the Río Bermejo, Argentina for two consecutive years. We measured changes in organic matter chemistry and in the rate of river bank erosion. We found that the Río Bermejo transports more organic matter sourced from mountains at periods of low flow, when the river does not erode its banks, and the river transports more organic matter sourced from floodplains during periods of high flow, when the river actively migrates. Because high flow periods account for most of the annual organic matter export, our results suggest that river-sourced organic matter in ocean basins is likely a mix of soil, sediment, and vegetation from floodplains.

Key Points:

- Discharge and river lateral migration rate set particulate organic carbon (POC) isotopic composition in a lowland river
- High lateral channel migration rates during the wet season drive replacement of headwater-sourced POC by floodplain POC
- Wet seasons account for ~85% of the annual POC export, suggesting that POC export is dominated by floodplain-sourced organic matter

Supporting Information:

Supporting Information may be found in the online version of this article.

Correspondence to:

N. Y. Golombek,
Nina.Golombek@dal.ca

Citation:

Golombek, N. Y., Scheingross, J. S., Repasch, M. N., Hovius, N., Menges, J., Sachse, D., et al. (2021). Fluvial organic carbon composition regulated by seasonal variability in lowland river migration and water discharge. *Geophysical Research Letters*, *48*, e2021GL093416. https://doi.org/10.1029/2021GL093416

Received 18 MAR 2021
Accepted 29 OCT 2021

Author Contributions:

Conceptualization: Nina Y. Golombek, Joel S. Scheingross, Niels Hovius, Dirk Sachse
Data curation: Nina Y. Golombek
Formal analysis: Nina Y. Golombek, Joel S. Scheingross, Maarten Lupker, Negar Haghipour, Simon R. Poulson, Darren R. Gröcke
Funding acquisition: Joel S. Scheingross, Niels Hovius, Dirk Sachse
Investigation: Nina Y. Golombek, Marisa N. Repasch, Niels Hovius, Dirk Sachse, Francisco G. Latosinski

1. Introduction

Burial of particulate organic carbon (POC) in sedimentary basins drives a long-term atmospheric CO_2 sink (e.g., France-Lanord & Derry, 1997) and creates paleoclimate archives (e.g., Hein et al., 2017). However, POC flux to depositional basins, and the paleoclimate conditions recorded therein, can be modulated during source to sink transit, analogous to how fluvial transport modifies environmental signals in clastic deposits (Hajek & Straub, 2017; Jerolmack & Paola, 2010). In lowland rivers, sediment exchange between rivers and floodplains can modify upstream-derived POC (Aufdenkampe et al., 2007; Galy et al., 2008; Moreira-Turcq et al., 2013; Torres et al., 2017). Floodplains store, modify, and oxidize upstream-derived POC (Bouchez et al., 2010; Scheingross et al., 2019, 2021), and floodplain vegetation provide an additional POC source (e.g., Lininger et al., 2018; Moreira-Turcq et al., 2013; Sutfin et al., 2016).

The fate of POC in lowland rivers has implications for the carbon cycle and the creation of paleoclimate archives. POC sourced from sedimentary rock (i.e., petrogenic POC, POC_{petro}) may be oxidized during floodplain

Methodology: Nina Y. Golombek, Marisa N. Repasch, Johanna Menges
Project Administration: Joel S. Scheingross, Niels Hovius
Resources: Maarten Lupker, Timothy I. Eglinton, Negar Haghipour, Simon R. Poulson, Darren R. Gröcke, Francisco G. Latosinski, Ricardo N. Szupiany
Software: Johanna Menges
Supervision: Joel S. Scheingross
Validation: Nina Y. Golombek
Visualization: Nina Y. Golombek
Writing – original draft: Nina Y. Golombek, Joel S. Scheingross
Writing – review & editing: Nina Y. Golombek, Joel S. Scheingross, Marisa N. Repasch, Niels Hovius, Johanna Menges, Dirk Sachse, Maarten Lupker, Timothy I. Eglinton, Negar Haghipour, Simon R. Poulson, Darren R. Gröcke, Francisco G. Latosinski, Ricardo N. Szupiany

storage and resuspension (Bouchez et al., 2010; Scheingross et al., 2021), producing a long-term atmospheric CO_2 source. However, this CO_2 source can be balanced by the long-term burial of recently produced POC (biospheric POC, POC_{bio}) sourced from channel margins and floodplains (Galy et al., 2007a). Furthermore, as paleoclimate information recorded in POC isotopic composition is often sensitive to the elevation at which POC was produced (e.g., Hoffmann et al., 2016; Ponton et al., 2014), replacement of headwater-sourced POC_{petro} with floodplain-sourced POC (including both *in situ* vegetation growth and soil development in the floodplain, and POC sourced in headwaters but modified during floodplain storage) complicates paleoclimate interpretations.

POC modification studies in lowland rivers have focused on sampling material transported at high discharges (e.g., Aufdenkampe et al., 2007; Bouchez et al., 2010; Galy et al., 2008) and examination of floodplain deposits formed during high flow (e.g., Goñi et al., 2014; Scheingross et al., 2021; Torres et al., 2020). However, POC composition varies seasonally, reflecting changes in headwater erosion (Clark et al., 2017; Goñi et al., 2013; Hemingway et al., 2017; Hilton et al., 2008; Li et al., 2015; Qu et al., 2020) and river-floodplain hydrologic connectivity (e.g., Moreira-Turcq et al., 2013; Pedrozo & Bonetto, 1987). Some of this variability may be driven by channel migration, which can regulate POC composition by setting the exchange of material between the rivers and floodplains and setting the timescales of vegetation growth (e.g., Lininger & Wohl, 2019; Torres et al., 2017). No study, to our knowledge, has explicitly explored the interplay between channel migration and seasonal variation in POC composition.

We hypothesize that the relative proportion of floodplain-sourced versus headwater-sourced POC in lowland rivers depends on channel migration rate and channel length, as lateral migration allows erosion of floodplain-sourced POC while headwater-sourced POC is deposited. This should lead to seasonal variability in POC composition. At high flow, lowland rivers should preferentially export floodplain-sourced POC due to increased channel migration rates (Constantine et al., 2014) and overbank flow, while at low flow, reduced channel migration rates limit bank erosion, allowing a greater representation of headwater-sourced POC (including POC_{petro}) in the river load. We test this hypothesis via analyzing POC composition for 2 years of suspended sediment in the Río Bermejo, Argentina.

2. Study Site

The Río Bermejo, Argentina drains the central Andes, and has headwaters underlain by Paleozoic marine and Cenozoic terrestrial sedimentary rocks (McGlue et al., 2016). At the mountain front, the Río San Francisco (RSF) joins the Río Bermejo to form the "Lowland Bermejo" (Figure 1), which runs ~1,270 km to the Río Paraguay with no tributary inputs (a paleochannel, the Río Bermejito, contributes <2% and <0.02% of Lowland Bermejo water and sediment discharge, respectively (Orfeo, 2006; Argentina National System of Hydrologic Information, *SNIH*, Figure 1). Both the Río Bermejo headwaters and lowlands have predominately C_3 vegetation (Powell & Still, 2009, Figure 1b). The Bermejo headwaters (drainage area of 1.2×10^5 km^2) and lowlands receive ~1,200 mm/yr and ~700 mm/yr precipitation, respectively (Harris et al., 2014), resulting in mean annual water discharge (Q_w) and sediment flux of 432 m^3/s and ~80 Mt/yr, respectively. River discharge and suspended sediment flux from January to April average ~750 m^3/s and ~410 kt/day in the Lowland Bermejo, respectively, ~5 times greater than average discharge and sediment flux during the June to December dry season of ~150 m^3/s and 15 kt/day, respectively (Figure 2) (Alarcón et al., 2003; Cafaro et al., 2010; Drago & Amsler, 1988; Repasch et al., 2020; *SNIH*). The Lowland Bermejo migrates across its floodplain at rates of ~6–23 m/yr, and experiences periodic avulsions (Page, 1889; Repasch et al., 2020). This exchange between the active river channel and its floodplain results in an average sediment transit time of ~8.4 ± 2.2 ky across the Lowland Bermejo (Repasch et al., 2020).

Organic matter in the Río Bermejo is sourced primarily from erosion of sedimentary bedrock, soil, floodplain sediment, and vegetation (Scheingross et al., 2021); high turbidity minimizes aquatic primary production (Pedrozo & Bonetto, 1987). POC_{petro} concentrations in Lowland Bermejo suspended sediment are low (~0.01–0.04%) relative to the total POC concentration (~0.01–1%), with no detectable downstream POC_{petro} changes (Scheingross et al., 2021). Analysis of an ~20 ky chronosequence of Lowland Bermejo floodplain sediments (up to 4.9 m depth) shows a systematic ^{13}C enrichment in POC with floodplain storage time, but no systematic variation in radiocarbon composition or nitrogen to carbon (N/OC) ratios (Scheingross et al., 2021).

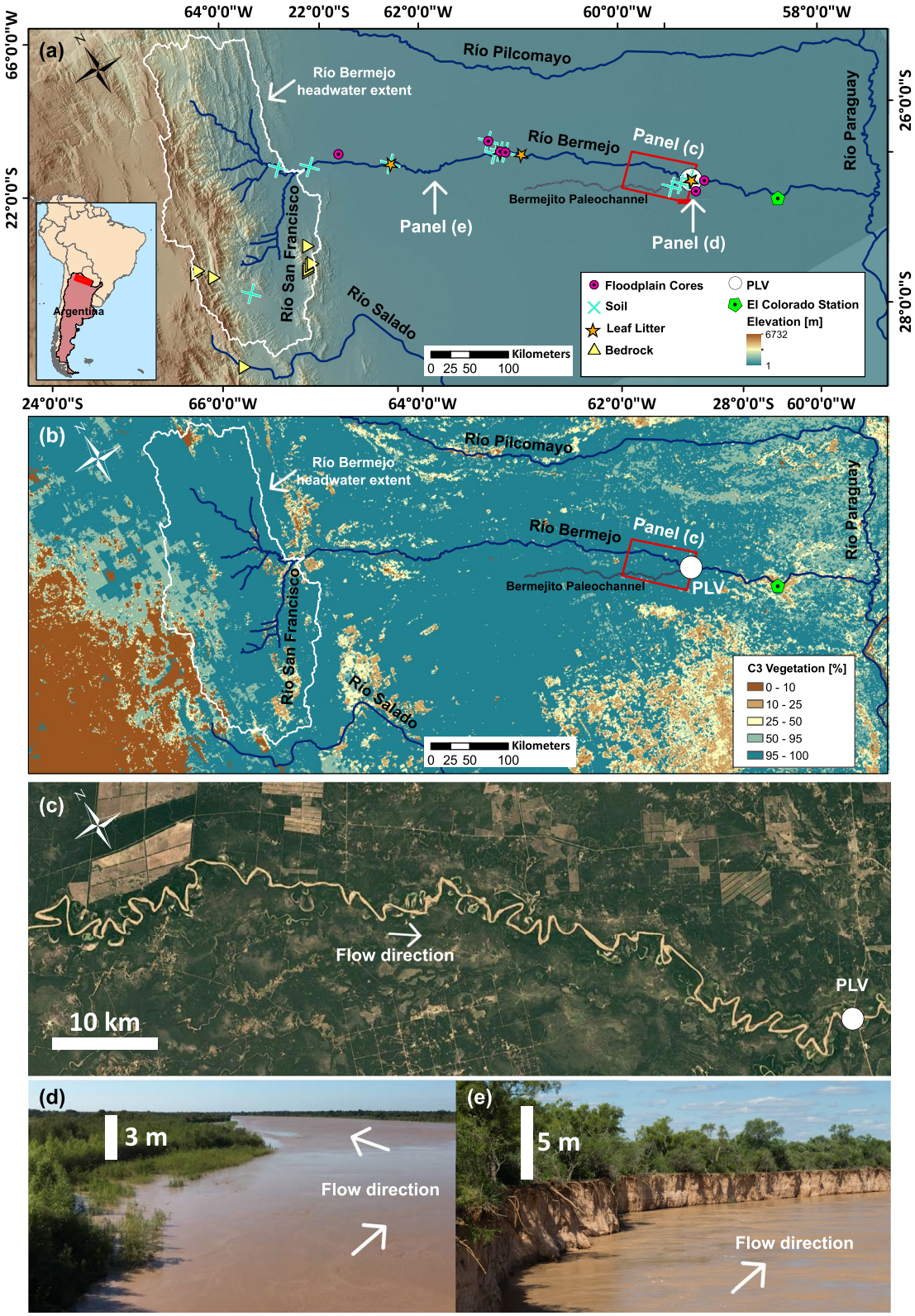

Figure 1. (a) Río Bermejo sampling locations. Red box denotes the area of channel migration rate measurements and corresponds to the panel (c) spatial extent, inset shows regional location. (b) C_3 vegetation percent (Powell et al., 2012). (c) Satellite imagery showing oxbow lakes and active channel migration. (d, e) Photos at Puente Lavalle (PLV) and ~450 km upstream of PLV, respectively.

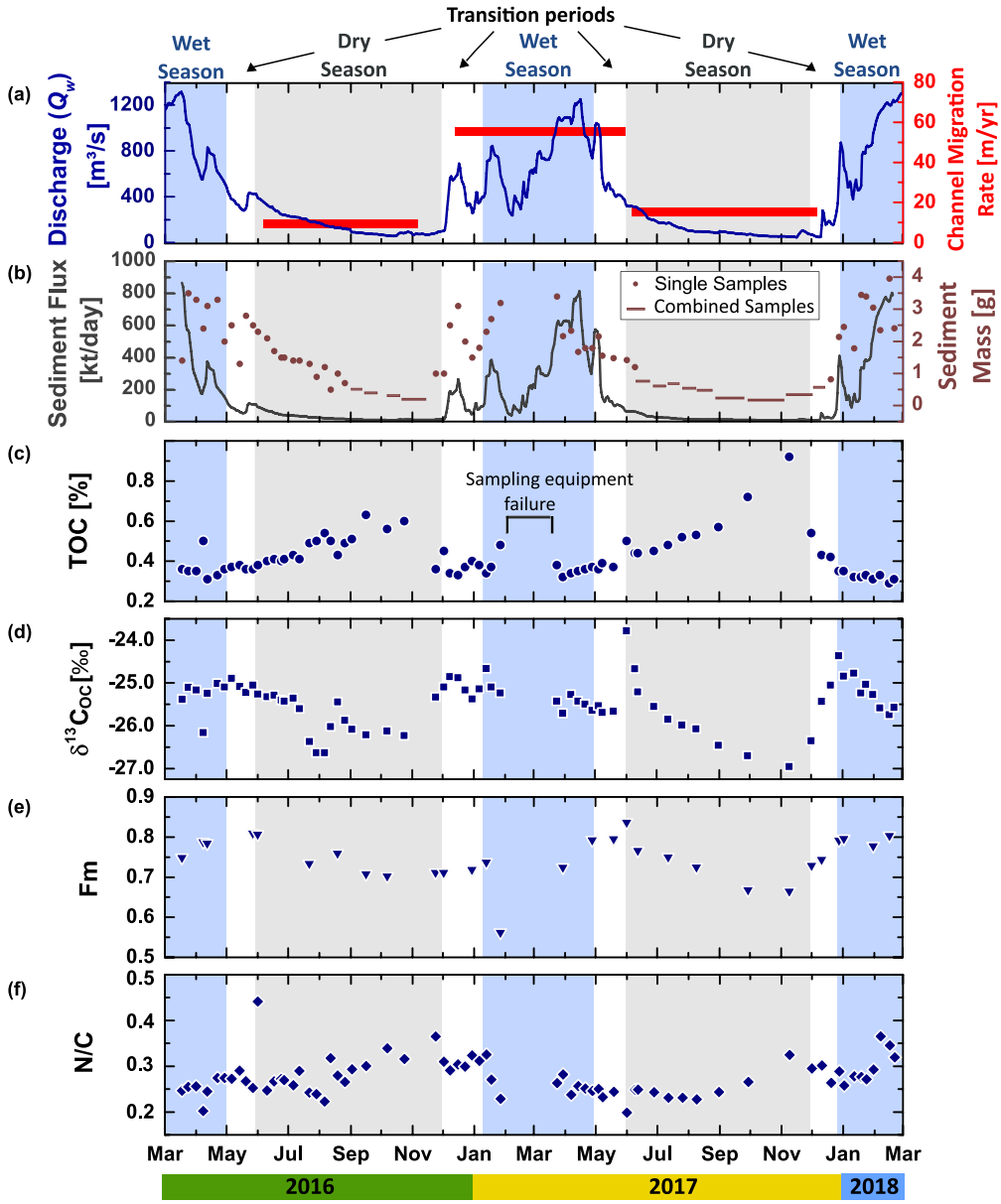

Figure 2. Temporal variation of (a) water discharge (measured at El Colorado by *SNIH*) and channel migration (bar length represents the time between satellite images), (b) sediment flux and mass collected, dots and lines represent single and amalgamated samples, respectively (Supplementary Text), (c) total organic carbon (TOC), (d) $\delta^{13}C_{OC}$, (e) Fm, and (f) N/OC.

3. Methods

3.1. Sample Collection

We evaluated POC temporal variability via collecting weekly suspended sediment samples (March 2016 to March 2018) at Puente Lavalle (PLV), ~870 river km downstream of the mountain front (Figure 1 and Table S1). We collected surface water samples (from a bridge using a river-rinsed bucket) to assess temporal POC variability without added complications due to POC variability with water column depth (e.g., Bouchez et al., 2014). Samples were filtered through a 0.22 µm polyethersulfone membrane, placed in *Whirl-PAK* bags, and stored on site at ambient temperatures for <1 year in a sealed, opaque box (with no visible mold growth), before transfer to Germany and storage at ~4 °C.

To document distinct POC sources, we collected 15 soil and 13 leaf litter samples (predominantly C_3 vegetation) from the Lowland Bermejo basin, and 10 bedrock (predominantly silt and mudstones) and 2 soil samples from the Río Bermejo headwaters (Figure 1 and Table S2). We collected leaf litter (at the ground surface) and soil (<5 cm from the ground surface) using an ethanol-rinsed trowel. We supplemented these samples with existing Río Bermejo floodplain sediment cores and headwater suspended sediment (Scheingross et al., 2021; Table S2).

3.2. Analytical Methods

We rinsed suspended sediment samples from filters into precombusted glass evaporating dishes using ultrapure (18.2 MΩ) water. Samples were oven-dried at 40 °C for >48 hr and we manually removed plant matter >1 cm. We homogenized suspended sediment and soil in an agate mortar without crushing, shredded leaf litter in a blender, and pulverized bedrock in a disc mill. Geochemical and grain size analyses required >0.8 g sediment; for samples <0.8 g, we combined consecutive weekly suspended samples to create a combined sample of >0.8 g (Table S1).

We split samples into aliquots for grain size analysis via laser diffraction (Supplementary Text) and geochemical analyses, and ground the latter to <63 μm. We further split the homogenized suspended sediment, bedrock, soil, and leaf litter aliquots for total nitrogen measurement (TN, wt %) and organic carbon analyses including total organic carbon (TOC, wt%), stable carbon isotope composition ($\delta^{13}C_{OC}$), and radiocarbon fraction modern (Fm). We decarbonated the aliquots for POC measurements using a liquid HCl leach (Galy et al., 2007b). TOC and TN were measured with an elemental analyzer (EA), and $\delta^{13}C_{OC}$ measured with a coupled EA-isotope ratio mass spectrometer (Supplementary Text). Radiocarbon was measured for 29 samples with an EA coupled to an accelerator mass spectrometer (McIntyre et al., 2017; Supplementary Text).

3.3. Channel Migration Rates

We measured lateral channel migration along a 140 km reach upstream of PLV (Figure 1c), which is the average distance required for the suspended load to be replaced with floodplain material via channel migration during high flow (Supplementary Text). We used Sentinel-2 and Planet satellite images (10 and 3 m resolution, respectively) to measure channel migration rates (Supplementary Text and Figure S1). We calculated the average lateral migration rate (E_{lat}) as (Torres et al., 2017):

$$E_{lat} = \left(\frac{A}{L \times t}\right) \quad (1)$$

where A is the eroded area measured from satellite images, L is channel length along which erosion was measured, and t is the time between images (estimated error of ~2 pixels which is ~20 m and equivalent to ~5–13% of the 150–400 m wide channel).

3.4. Data Analysis

We separated the wet and dry seasons at $Q_w = 400$ m³/s, based on the maximum observed dry season discharge in the study period and previously documented changes in the relation between suspended sediment flux and discharge (Alarcón et al., 2003, Figure 2). We quantified seasonal variability in POC composition by evaluating linear correlations between water discharge (Q_w) and TOC, $\delta^{13}C_{OC}$, Fm, and N/OC (wt %/wt %), for both the wet and dry seasons. We assessed statistical significance (defined at $p < 0.05$) using the Pearson correlation coefficient, ρ, where $\rho = 1$ and $\rho = -1$ for perfectly monotonic positive and negative correlations, respectively. We additionally tested for statistical differences between the populations of values in the wet and dry seasons using a two-sample Kolmogorov-Smirnov test (Massey, 1951).

We performed mixing analyses to assess relations between seasonal variation in POC composition and changes in the relative proportions of headwater-sourced and floodplain-sourced POC. We assume four possible POC endmembers: leaf litter, soil (i.e., organic-rich soil developed within the top 5 cm of the floodplain surface), aged floodplain sediment (deposits older than 100 years and from material >50 cm depth), and bedrock. Both leaf litter and soil can be sourced from the headwaters and floodplains, therefore, the presence of these endmembers is not diagnostic of either headwater-sourced or floodplain-sourced POC. In contrast, bedrock-derived POC_{petro} originates exclusively in the Río Bermejo headwaters (although POC_{petro} can be transiently stored in the Lowland

Bermejo floodplain during source to sink transport), while aged floodplain sediment comes primarily from the Lowland Bermejo, allowing us to use these endmembers as proxies for the relative contributions of headwater and floodplain-sourced POC. To determine the contributions of endmembers to the POC in the suspended sediment samples, we used MixSIAR, an open-source Bayesian tracer mixing model framework (Stock et al., 2018) which provides a probabilistic solution to endmember mixing. MixSIAR assumes geochemical tracers (e.g., N/OC, $\delta^{13}C_{OC}$, and Fm) are conserved in the mixing process and that tracer composition is known and invariant. MixSIAR allows for correlation between tracers and integrates the observed variability in endmember and mixture composition (Moore & Semmens, 2008; Parnell et al., 2013; Stock et al., 2018), and has been used for fluvial POC (Blake et al., 2018; Menges et al., 2020). We parameterized MixSIAR using TOC-weighted means and standard deviations of N/OC, $\delta^{13}C_{OC}$, Fm for each endmember. We ran calculations for samples with measurements of N/OC, $\delta^{13}C_{OC}$, and Fm, and grouped suspended sediments into five discharge bins of >9 samples (Q_w < 100 m³/s, 100 < Q_w < 200 m³/s, 200 < Q_w < 400 m³/s, 400 < Q_w < 800 m³/s, Q_w > 800 m³/s). We used an uninformative prior, ran each model with a chain length of 10^6 and tested its convergence with Gelman-Rubin (Gelman & Rubin, 1992) and Geweke Diagnostics (Geweke, 1991). Models reached convergence after runs with 3×10^5 iterations, a burn-in of 2×10^5, and 3 chains.

4. Results

4.1. Water Discharge, Sediment Mass and Channel Migration Rates

Water discharge varied from 45 to 1,300 m³/s over the study period and was positively correlated with suspended sediment sample mass (Figures 2a and 2b). We assessed grain size using the median grain diameter (D_{50}) and fraction of grains <2 μm (f_2, Scheingross et al., 2021). D_{50} and f_2 of surface water samples varied from 3 to 6 μm and 0.12 to 0.70, respectively, with no systematic seasonal trends (Table S1).

Channel migration rates increased from ~13 to 15 m/yr in the dry season to ~55 m/yr in the wet season, ~10× faster than average migration rates for rivers with vegetated banks of similar width (Ielpi & Lapôtre, 2020). Erosion occurred predominately on the outer side of channel bends in the wet season; we observed no systematic relationship between channel curvature and dry season erosion (Figure S1). Migration rates were typically <30 m (near our detection limit using Sentinel-2 imagery, Supplementary Text) along the entire channel length in the dry season, and along portions of the channel during the wet season. Therefore, both migration rate estimates likely include mapping errors and overestimate the true migration.

4.2. Seasonal POC Variation

Suspended sediment TOC ranged from 0.32% to 0.92% (Figures 2c and 3a, Table S1). For the dry season (Q_w < 400 m³/s), TOC had a statistically significant negative correlation with discharge ($\rho = -0.64$, $p < 10^{-5}$) (Figure 3a). While in the wet season (Q_w > 400 m³/s), TOC averaged 0.35% ± 0.06%, showing no statistically significant correlation with discharge ($\rho = -0.30$, $p = 0.11$, Figure 3a). Temporal TOC changes were gradual, typically increasing from the middle of the wet season until the end of the dry season (Figure 2c). We also observed a statistically significant correlation between D_{50} and TOC ($p = 0.01$) and a suggestive correlation between f_2 and TOC ($p = 0.06$); however, there is no statistically significant correlation between either D_{50} or f_2 and water discharge (Figure S6), likely because we sampled only surface water, thereby limiting grain size variations.

Suspended sediment $\delta^{13}C_{OC}$ values ranged from −26.9‰ to −24.3‰ (Figures 2d and 3b, Table S1). For Q_w < 400 m³/s, $\delta^{13}C_{OC}$ showed a statistically significant linear correlation with discharge ($\rho = 0.71$, $p < 10^{-7}$, Figure 3b). For Q_w > 400 m³/s, $\delta^{13}C_{OC}$ varied between −26.1‰ and −24.6‰ with no statistically significant correlation with discharge ($\rho = -0.32$, $p = 0.08$, Figure 3b). Temporal variation in $\delta^{13}C_{OC}$ values were gradual, with occasional spikes (e.g., June 2017, Figure 2d).

Fm ranged from 0.66 to 0.83 (with one outlier, Fm = 0.56, Figures 2e and 3c, Table S1). During the dry season, Fm and Q_w showed a statistically significant positive linear correlation with discharge ($\rho = 0.80$, $p < 10^{-4}$, Figure 3c). In the wet season, Fm remained approximately constant, showing no significant correlation with discharge ($\rho = 0.02$, $p = 0.95$, Figure 3c). N/OC ratios varied between 0.2 and 0.44, with no significant correlation between N/OC and discharge (Figure 3d and Table S1) and did not show consistent temporal variations (Figure 2f).

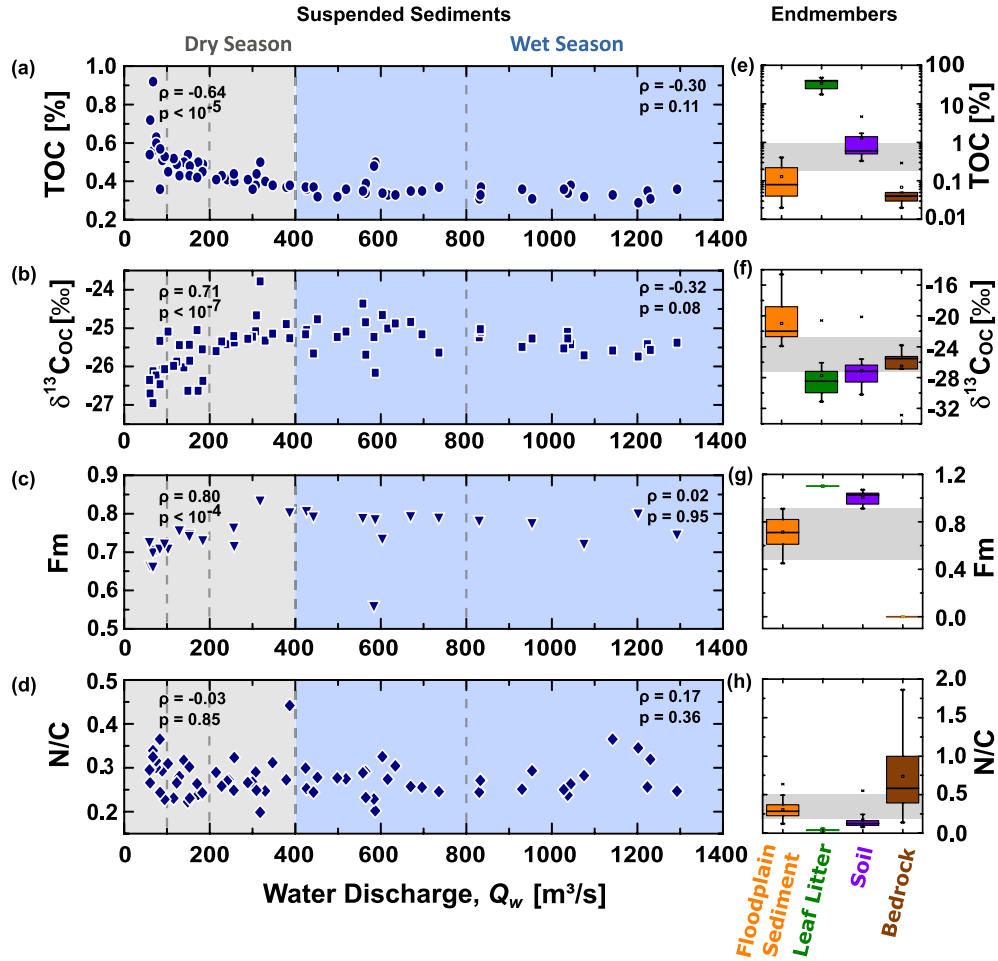

Figure 3. Variations in suspended sediment (a) total organic carbon (TOC), (b) $\delta^{13}C_{OC}$, (c) Fm, and (d) N/OC as a function of water discharge at Puente Lavalle (PLV). ρ and p are the Pearson correlation coefficient and significance level, respectively. Dashed lines represent discharge bins used in Figure 4. (e–h) Endmember boxplots; boxes show interquartile range and mean with whiskers corresponding to the 95th and 5th percentile of measured values. Gray shading shows (a–d) extent.

4.3. Endmember Contributions

Endmember POC sources showed partial overlap in measured values of TOC, $\delta^{13}C_{OC}$, Fm, and N/OC (Figures 3e–3h and S2). We set Fm = 1.1 for leaf litter and measurements displayed 0.02 < N/OC < 0.06 and −31‰ < $\delta^{13}C_{OC}$ < −21‰. Soil measurement ranged from 0.09 < N/OC < 0.55, −30‰ < $\delta^{13}C_{OC}$ < −20‰, and 0.9 < Fm < 1, while floodplain sediment showed 0.15 < N/OC < 0.5, −23‰ < $\delta^{13}C_{OC}$ < −14‰, and 0.5 < Fm < 0.9. Bedrock had 0.14 < N/OC < 2, −32.9‰ < $\delta^{13}C_{OC}$ < −23.8‰, and was set to Fm = 0 by definition (Tables S2 and S3). MixSIAR posterior distributions of endmember contributions to the total POC load were broader for leaf litter and soil than floodplain sediment and bedrock, reflecting the more similar isotopic composition of the former (Figure 4a and Table S2). The floodplain sediment contribution increases with discharge, reaching a maximum mean value of 44% at 400 < Q_w < 800 m³/s, while the contribution from bedrock decreases with discharge, reaching a minimum of 13% at 400 < Q_w < 800 m³/s. Posterior distributions of soil and leaf litter remain approximately constant with discharge (Figure 4a). These results agree with the mixing diagrams (Figure S2) which show that dry season samples (Q_w < 400 m^3/s) generally have lower Fm and $\delta^{13}C_{OC}$ values than wet season samples (Q_w > 400 m^3/s).

We estimated the contribution of individual endmembers to the overall OC flux by multiplying the mean value of its posterior distributions by the POC flux (Supplementary Text S3) for a given discharge bin (Figure 4b). The soil endmember dominates the POC flux throughout all discharges, while the floodplain endmember has high contributions in the wet seasons and is overtaken by the bedrock endmember in the dry seasons. We also compared

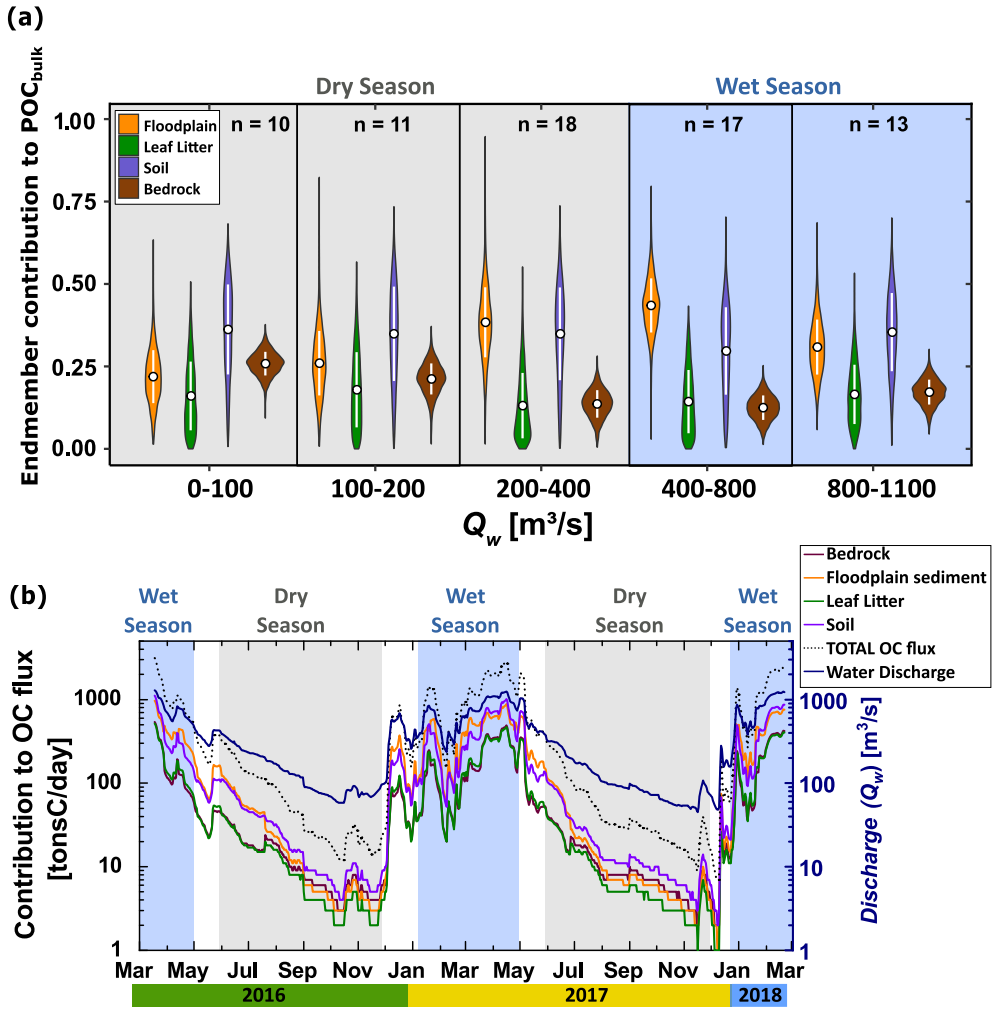

Figure 4. MixSIAR-derived contributions of soil, leaf litter, floodplain sediment, and bedrock endmembers to the bulk particulate organic carbon (POC) load. (a) Full posterior distributions; white dots and centerlines represent posterior mean and standard deviation, respectively; *n* denotes the number of samples per discharge bin. (b) Temporal variation in endmember contributions to the OC flux.

suspended sediment collected at the PLV monitoring station with samples previously collected ~900 km upstream at the mountain front (Scheingross et al., 2021), which provide an approximation of the bulk headwater POC composition. Mountain front samples and suspended sediment collected in the dry season at PLV overlap in $\delta^{13}C_{OC}$ and N/OC values, but mountain front samples have slightly higher Fm values than suspended sediment at PLV (Figure S2).

5. Discussion

5.1. Seasonal Variation of POC Source

Our results suggest that compositional changes in POC with increasing discharge reflect increasing proportions of floodplain-sourced POC relative to (headwater-sourced) POC_{petro} (Figures 4a and 4b). Our analysis of the MixSIAR results relies heavily on relative changes in the posterior distributions of POC_{petro} and aged floodplain sediment POC, because the relatively uniform C_3 vegetation throughout the catchment suggests that both headwater-sourced and floodplain-sourced leaf litter and soil are likely to have similar compositions. Our estimates of the headwater-derived OC flux is therefore likely a minimum estimate, as it does not include the headwater OC_{bio} component. The MixSIAR results indicate that POC samples depleted in ^{13}C in the dry season primarily reflect soil and bedrock contributions, with lesser contributions from floodplain sediment and leaf litter (Figures 4a

and 4b). This implies that the Bermejo is most efficient in transporting headwater-sourced POC in the dry season, consistent with the agreement between $\delta^{13}C_{OC}$ and N/OC values of suspended sediment collected at the mountain front and dry season suspended sediment collected downstream at PLV (Figure S2). Headwater-sourced POC contributions likely increase in the dry season because low discharge limits channel bank erosion, thereby reducing the input of floodplain-sourced POC. The relative enrichment in ^{13}C and ^{14}C for POC from ~100 to 800 m^3/s reflects an increase in floodplain sediment and decrease in POC_{petro} (Figure 3), and likely results from increased channel migration rates. For Q_w > 800 m^3/s, MixSIAR results show that the floodplain sediment POC contribution is slightly lower and bedrock POC contribution is slightly higher than those calculated for the 400–800 m^3/s bin (Figure 4a). This could reflect the lofting of POC_{petro}-enriched bed material to the water surface at very high discharges; however, floodplain-sourced POC still remains a larger contribution to the total POC load than at low discharges, consistent with our hypothesis that increased discharge increases the representation of floodplain-sourced POC in the fluvial load.

The seasonal variation in floodplain-sourced relative to headwater-sourced POC is consistent with our observations of seasonally variable river lateral migration. Lateral channel migration allows for sediment deposition in point bars and the erosion of floodplain sediment from cut banks, such that the rate of lateral migration and the distance downstream from the mountain front should set the relative fraction of floodplain-sourced versus headwater-sourced POC. We interpret discharge-induced changes in lateral migration rate are more likely to set POC composition than the potential for discharge-induced changes in grain size, as we observe no statistical correlation between water discharge and grain size in our samples (Figure S6). Repasch et al. (2020) used decadal-averaged river migration rates to estimate that, on average, the sediment load of the Bermejo exchanges completely with the floodplain every ~280 km. This implies that most sediment reaching the PLV monitoring station, ~870 km downstream of the mountain front, has experienced ~3 cycles of floodplain deposition, transient storage, and re-erosion. We thus expect the vast majority of sediment passing the PLV station in the wet season (when lateral migration rates are high) to be floodplain-sourced, consistent with our geochemical observations. Conversely, in the dry season, limited sediment exchange between the channel and floodplain allows a greater fraction of headwater-sourced sediment to bypass PLV without floodplain storage. This implies that during low flows with negligible river-floodplain exchange, POC may travel from source to sink over days to weeks, whereas during high flow, exchange with the banks results in floodplain storage and transit times that can extend to millennia (Repasch et al., 2020).

5.2. Implications for POC Export to Depositional Basins

To explore how seasonal variability may affect POC composition delivered to basins, we estimated Río Bermejo POC export (Supplementary Text and Figure S5) using the 26-year daily water discharge record (*SNIH*), a Q_w-TOC rating curve (Figure S3) and a sediment flux versus water discharge rating curve (Figure S4). From dry to wet seasons there is a threefold decrease in POC concentration; however, the increase in sediment flux results in an ~100-fold increase in POC flux. Integrating over the 26-year daily discharge record, we estimate that the aged floodplain sediment flux is ~2.1 times greater than POC_{petro} flux, suggesting that floodplain-sourced POC dominates contributions to downstream sedimentary basins. We suggest that POC deposited in basins downstream of actively migrating rivers with large floodplains, such as the Río Bermejo, is likely to be sourced primarily from adjacent floodplains, and that the input of headwater material is likely to be overprinted before organic matter reaches its final sink. As sediment and POC can take order 10^3 yr to transit lowland rivers (Repasch et al., 2020; Wittmann et al., 2015), these results imply that paleoclimate information recorded in POC deposited downstream of lowland rivers is likely not sensitive to high frequency ($<10^3$ yr) climatic variations. Instead, high frequency climate signals and headwater-sourced POC may be better preserved in deposits of small mountain streams draining directly to the ocean.

6. Conclusions

Our data suggests that low channel migration rates cause the Río Bermejo to act as a conduit preferentially transporting headwater-sourced POC in the dry season, while in the wet season, high lateral channel migration rates drive significant influxes of floodplain POC into the river load that overprint the headwater signature. The wet season comprises ~85% of the total annual POC flux, suggesting that the majority of organic matter exported from the Bermejo derives from the lowlands. This work highlights how hydrologic variability sets the

composition of POC exported from lowland rivers, allowing improved interpretation of the provenance of organic material preserved in depositional centers.

Data Availability Statement

All data are accessible though the PANGAEA data repository (https://doi.org/10.1594/PANGAEA.932558), in Scheingross et al. (2021) and available for download from *SNIH* (Sistema Nacional de Información Hídrica, https://snih.hidricosargentina.gob.ar/).

Acknowledgments
We thank Birgit Plessen and Petra Maier for POC measurements made at GFZ, the Biogeoscience Group and the Laboratory for Ion Beam Physics, ETH Zurich, for AMS measurements, and Kristen Cook for channel migration assistance. We acknowledge funding from an Alexander von Humboldt Postdoctoral Fellowship (J.S.S.), the StRATEGy international research training group (D.S. and M.R.); Deutsche Forschungsgemeinschaft (DFG) grant STR 373/34–1, and the Helmholtz Association (N.H.). Open access funding enabled and organized by Projekt DEAL.

References

Alarcón, J. J., Szupiany Ricardo, N., Monagnini, M. D., Gaudin, H., Prendes, H. H., & Amsler, M. L. (2003). Evaluación del transporte de sedimentos en el tramo medio del Río Paraná. In *Primer Simposio Regional sobre Hidráulica de Ríos, Argentina: Ezeiza*.

Aufdenkampe, A. K., Mayorga, E., Hedges, J. I., Llerena, C., Quay, P. D., Gudeman, J., et al. (2007). Organic matter in the Peruvian headwaters of the Amazon: Compositional evolution from the Andes to the lowland Amazon mainstem. *Organic Geochemistry*, *38*(3), 337–364. https://doi.org/10.1016/j.orggeochem.2006.06.003

Blake, W. H., Boeckx, P., Stock, B. C., Smith, H. G., Bodé, S., Upadhayay, H. R., et al. (2018). A deconvolutional Bayesian mixing model approach for river basin sediment source apportionment. *Scientific Reports*, *8*(1), 1–12. https://doi.org/10.1038/s41598-018-30905-9

Bouchez, J., Beyssac, O., Galy, V., Gaillardet, J., France-Lanord, C., Maurice, L., & Moreira-Turcq, P. (2010). Oxidation of petrogenic organic carbon in the Amazon floodplain as a source of atmospheric CO_2. *Geology*, *38*(3), 255–258. https://doi.org/10.1130/G30608.1

Bouchez, J., Galy, V., Hilton, R. G., Gaillardet, J. Ô., Moreira-Turcq, P., Pérez, M. A., et al. (2014). Source, transport and fluxes of Amazon River particulate organic carbon: Insights from river sediment depth-profiles. *Geochimica et Cosmochimica Acta*, *133*, 280–298. https://doi.org/10.1016/j.gca.2014.02.032

Cafaro, E. D., Latrubesse, E. M., & Ramonell, C. G. (2010). Estimación De La Carga Sedimentaria Que Aportan Los Andes Y Sierras Asociadas Al Chaco Argentino—Paraguayo. In *XXIV Congreso Latinoamericano De Hidráulica Punta del Este, Uruguay* (p. 9).

Clark, K. E., Hilton, R. G., West, A. J., Robles Caceres, A., Gröcke, D. R., Marthews, T. R., et al. (2017). Erosion of organic carbon from the Andes and its effects on ecosystem carbon dioxide balance. *Journal of Geophysical Research: Biogeosciences*, *122*, 449–469. https://doi.org/10.1002/2016JG003615

Constantine, J. A., Dunne, T., Ahmed, J., Legleiter, C., & Lazarus, E. D. (2014). Sediment supply as a driver of river meandering and floodplain evolution in the Amazon Basin. *Nature Geoscience*, *7*(12), 899–903. https://doi.org/10.1038/ngeo2282

Drago, E. C., & Amsler, M. L. (1988). Suspended sediment at a cross section of the Middle Paraná River: Concentration, granulometry and influence of the main tributaries (IAHS Publ. No. 174, pp. 381–396). In *Sediment Budgets (Proceedings of the Porto Alegre Symposium.*

France-Lanord, C., & Derry, L. A. (1997). Organic carbon burial forcing of the carbon cycle from Himalayan erosion. *Nature*, *390*(6655), 65–67. https://doi.org/10.1038/36324

Galy, V., Bouchez, J., & France-Lanord, C. (2007). Determination of total organic carbon content and δ13C in carbonate-rich detrital sediments. *Geostandards and Geoanalytical Research*, *31*(3), 199–207. https://doi.org/10.1111/j.1751-908X.2007.00864.x

Galy, V., France-Lanord, C., Beyssac, O., Faure, P., Kudrass, H., & Palhol, F. (2007). Efficient organic carbon burial in the Bengal fan sustained by the Himalayan erosional system. *Nature*, *450*(7168), 407–410. https://doi.org/10.1038/nature06273

Galy, V., France-Lanord, C., & Lartiges, B. (2008). Loading and fate of particulate organic carbon from the Himalaya to the Ganga-Brahmaputra delta. *Geochimica et Cosmochimica Acta*, *72*(7), 1767–1787. https://doi.org/10.1016/j.gca.2008.01.027

Gelman, A., & Rubin, D. B. (1992). Inference from iterative simulation using multiple sequences. *Statistical Science*, *7*(4), 457–472. https://doi.org/10.1214/ss/1177011136

Geweke, J. (1991). *Evaluating the accuracy of sampling-based approaches to the calculation of posterior moments* (Staff Report 148). Federal Reserve Bank of Minneapolis.

Goñi, M. A., Hatten, J. A., Wheatcroft, R. A., & Borgeld, J. C. (2013). Particulate organic matter export by two contrasting small mountainous rivers from the Pacific Northwest, U.S.A. *Journal of Geophysical Research: Biogeosciences*, *118*, 112–134. https://doi.org/10.1002/jgrg.20024

Goñi, M. A., Moore, E., Kurtz, A., Portier, E., Alleau, Y., & Merrell, D. (2014). Organic matter compositions and loadings in soils and sediments along the Fly River, Papua New Guinea. *Geochimica et Cosmochimica Acta*, *140*, 275–296. https://doi.org/10.1016/j.gca.2014.05.034

Hajek, E. A., & Straub, K. M. (2017). Autogenic sedimentation in clastic stratigraphy. *Annual Review of Earth and Planetary Sciences*, *45*(1), 681–709. https://doi.org/10.1146/annurev-earth-063016-015935

Harris, I., Jones, P. D., Osborn, T. J., & Lister, D. H. (2014). Updated high-resolution grids of monthly climatic observations—The CRU TS3.10 Dataset. *International Journal of Climatology*, *34*, 623–642. https://doi.org/10.1002/joc.3711

Hein, C. J., Galy, V., Galy, A., France-Lanord, C., Kudrass, H., & Schwenk, T. (2017). Post-glacial climate forcing of surface processes in the Ganges-Brahmaputra river basin and implications for carbon sequestration. *Earth and Planetary Science Letters*, *478*, 89–101. https://doi.org/10.1016/j.epsl.2017.08.013

Hemingway, J. D., Schefuß, E., Spencer, R. G. M., Dinga, B. J., Eglinton, T. I., McIntyre, C., & Galy, V. V. (2017). Hydrologic controls on seasonal and inter-annual variability of Congo River particulate organic matter source and reservoir age. *Chemical Geology*, *466*, 454–465. https://doi.org/10.1016/j.chemgeo.2017.06.034

Hilton, R. G., Galy, A., & Hovius, N. (2008). Riverine particulate organic carbon from an active mountain belt: Importance of landslides. *Global Biogeochemical Cycles*, *22*, GB1017. https://doi.org/10.1029/2006GB002905

Hoffmann, B., Feakins, S. J., Bookhagen, B., Olen, S. M., Adhikari, D. P., Mainali, J., & Sachse, D. (2016). Climatic and geomorphic drivers of plant organic matter transport in the Arun River, E Nepal. *Earth and Planetary Science Letters*, *452*, 104–114. https://doi.org/10.1016/j.epsl.2016.07.008

Ielpi, A., & Lapôtre, M. G. A. (2020). A tenfold slowdown in river meander migration driven by plant life. *Nature Geoscience*, *13*(1), 82–86. https://doi.org/10.1038/s41561-019-0491-7

Jerolmack, D. J., & Paola, C. (2010). Shredding of environmental signals by sediment transport. *Geophysical Research Letters*, *37*, L19401. https://doi.org/10.1029/2010GL044638

Lininger, K. B., & Wohl, E. (2019). Floodplain dynamics in North American permafrost regions under a warming climate and implications for organic carbon stocks: A review and synthesis. *Earth-Science Reviews*, *193*, 24–44. https://doi.org/10.1016/j.earscirev.2019.02.024

Lininger, K. B., Wohl, E., & Rose, J. R. (2018). Geomorphic controls on floodplain soil organic carbon in the Yukon Flats, Interior Alaska, from reach to River Basin Scales. *Water Resources Research*, *54*, 1934–1951. https://doi.org/10.1002/2017WR022042

Li, G., Wang, X. T., Yang, Z., Mao, C., West, A. J., & Ji, J. (2015). Dam-triggered organic carbon sequestration makes the Changjiang (Yangtze) river basin (China) a significant carbon sink. *Journal of Geophysical Research: Biogeosciences*, *120*, 39–53. https://doi.org/10.1002/2014JG002646

Massey, F. J. (1951). The Kolmogorov-Smirnov test for goodness of fit. *Journal of the American Statistical Association*, *46*(253), 68–78. https://doi.org/10.1080/01621459.1951.10500769

McGlue, M. M., Smith, P. H., Zani, H., Silva, A., Carrapa, B., Cohen, A. S., & Pepper, M. B. (2016). An integrated sedimentary systems analysis of the RíO Bermejo (Argentina): Megafan character in the overfilled Southern Chaco Foreland Basin. *Journal of Sedimentary Research*, *86*(12), 1359–1377. https://doi.org/10.2110/jsr.2016.82

McIntyre, C. P., Wacker, L., Haghipour, N., Blattmann, T. M., Fahrni, S., Usman, M., et al. (2017). Online ^{13}C and ^{14}C gas measurements by EA-IRMS-AMS at ETH Zürich. *Radiocarbon*, *59*(3), 893–903. https://doi.org/10.1017/RDC.2016.68

Menges, J., Hovius, N., Andermann, C., Lupker, M., Haghipour, N., Märki, L., & Sachse, D. (2020). Variations in organic carbon sourcing along a trans-Himalayan river determined by a Bayesian mixing approach. *Geochimica et Cosmochimica Acta*, *286*, 159–176. https://doi.org/10.1016/j.gca.2020.07.003

Moore, J. W., & Semmens, B. X. (2008). Incorporating uncertainty and prior information into stable isotope mixing models. *Ecology Letters*, *11*(5), 470–480. https://doi.org/10.1111/j.1461-0248.2008.01163.x

Moreira-Turcq, P., Bonnet, M. P., Amorim, M., Bernardes, M., Lagane, C., Maurice, L., et al. (2013). Seasonal variability in concentration, composition, age, and fluxes of particulate organic carbon exchanged between the floodplain and Amazon River. *Global Biogeochemical Cycles*, *27*, 119–130. https://doi.org/10.1002/gbc.20022

Orfeo, O. (2006). Dynamics of sediment transport in two subtropical plain rivers of South America. *Zeitschrift Fur Geomorphologie, Supplementband*, *145*, 229–241.

Page, J. (1889). The Gran Chaco and its rivers. *Proceedings of the Royal Geographical Society and Monthly Record of Geography*, *11*(3), 129–152. https://doi.org/10.2307/1801354

Parnell, A. C., Phillips, D. L., Bearhop, S., Semmens, B. X., Ward, E. J., Moore, J. W., et al. (2013). Bayesian stable isotope mixing models. *Environmetrics*, *24*(6), 387–399. https://doi.org/10.1002/env.2221

Pedrozo, F., & Bonetto, C. (1987). Nitrogen in the and phosphorus River (South transport America) Bermejo. *Revue d'Hydrobiologie Tropicale*, *20*(2), 91–99.

Ponton, C., West, A. J., Feakins, S. J., & Galy, V. (2014). Leaf wax biomarkers in transit record river catchment composition. *Geophysical Research Letters*, *41*, 6420–6427. https://doi.org/10.1002/2014GL061328

Powell, R. L., & Still, C. J. (2009). *Biogeography of C3 and C4 vegetation on South America* (pp. 2935–2942). Anais XIV Simpósio Brasileiro de Sensoriamento Remoto.

Powell, R. L., Yoo, E.-H., & Still, C. J. (2012). Vegetation and soil carbon-13 isoscapes for South America: Integrating remote sensing and ecosystem isotope measurements. *Ecosphere*, *3*(11), 109. https://doi.org/10.1890/es12-00162.1

Qu, Y., Jin, Z., Wang, J., Wang, Y., Xiao, J., Gou, L. F., et al. (2020). The sources and seasonal fluxes of particulate organic carbon in the Yellow River. *Earth Surface Processes and Landforms*, *45*(9), 2004–2019. https://doi.org/10.1002/esp.4861

Repasch, M., Scheingross, J. S., Sachse, D., Szupiany Ricardo, N., Wittmann, H., Orfeo, O., et al. (2020). Sediment transit time and floodplain storage dynamics in alluvial rivers revealed by meteoric 10Be. *Journal of Geophysical Research: Earth Surface*, *125*, e2019JF005419. https://doi.org/10.1029/2019JF005419

Scheingross, J. S., Hovius, N., Dellinger, M., Hilton, R. G., Repasch, M., Sachse, D., et al. (2019). Preservation of organic carbon during active fluvial transport and particle abrasion. *Geology*, *47*(10), 958–962. https://doi.org/10.1130/G46442.1

Scheingross, J. S., Repasch, M. N., Hovius, N., Sachse, D., Lupker, M., Fuchs, M., et al. (2021). The fate of fluvially-deposited organic carbon during transient floodplain storage. *Earth and Planetary Science Letters*, *561*, 116822. https://doi.org/10.1016/j.epsl.2021.116822

Sistema Nacional de Información Hídrica (SNIH). Ministerio de Obras Públicas Argentina. Retrieved from https://snih.hidricosargentina.gob.ar/

Stock, B. C., Jackson, A. L., Ward, E. J., Parnell, A. C., Phillips, D. L., & Semmens, B. X. (2018). Analyzing mixing systems using a new generation of Bayesian tracer mixing models. *PeerJ*, *6*, e5096. https://doi.org/10.7717/peerj.5096

Sutfin, N. A., Wohl, E. E., & Dwire, K. A. (2016). Banking carbon: A review of organic carbon storage and physical factors influencing retention in floodplains and riparian ecosystems. *Earth Surface Processes and Landforms*, *41*(1), 38–60. https://doi.org/10.1002/esp.3857

Torres, M. A., Kemeny, P. C., Lamb, M. P., Cole, T. L., & Fischer, W. W. (2020). Long-term storage and age-biased export of fluvial organic carbon: Field evidence from West Iceland. *Geochemistry, Geophysics, Geosystems*, *21*, e2019GC008632. https://doi.org/10.1029/2019GC008632

Torres, M. A., Limaye, A. B., Ganti, V., Lamb, M. P., Joshua West, A., & Fischer, W. W. (2017). Model predictions of long-lived storage of organic carbon in river deposits. *Earth Surface Dynamics*, *5*(4), 711–730. https://doi.org/10.5194/esurf-5-711-2017

Wittmann, H., Von Blanckenburg, F., Dannhaus, N., Bouchez, J., Gaillardet, J., Guyot, J. L., et al. (2015). A test of the cosmogenic 10Be(meteoric)/9Be proxy for simultaneously determining basin-wide erosion rates, denudation rates, and the degree of weathering in the Amazon basin. *Journal of Geophysical Research: Earth Surface*, *120*, 2498–2528. https://doi.org/10.1002/2015JF003581

Geophysical Research Letters

Supporting Information for

Fluvial organic carbon composition regulated by seasonal variability in lowland river migration and water discharge

Nina Y. Golombek[1,2,3], Joel S. Scheingross[1,4], Marisa N. Repasch[1,5], Niels Hovius[1,2], Johanna Menges[1,6], Dirk Sachse[1], Maarten Lupker[7], Timothy I. Eglinton[7], Negar Haghipour[7,8], Simon R. Poulson[4], Darren R. Gröcke[9], Francisco G. Latosinski[10,11], Ricardo N. Szupiany[10,11]

[1]GFZ - German Research Centre for Geosciences, Potsdam, GERMANY
[2]Department of Geosciences, University of Potsdam, GERMANY
[3]Department of Earth and Environmental Sciences, Dalhousie University, Halifax, CANADA
[4]Department of Geological Sciences and Engineering, University of Nevada, Reno, USA
[5]Lawrence Livermore National Lab, Livermore, USA
[6]MARUM - Center for Marine Environmental Sciences, University of Bremen, Bremen, GERMANY
[7]Geological Institute, ETH Zürich, SWITZERLAND
[8]Laboratory of Ion Beam Physics, ETH Zürich, SWITZERLAND
[9]Department of Earth Sciences, Durham University, UK
[10]National Council for Scientific and Technological Research (CONICET), ARGENTINA
[11]School of Engineering and Water Sciences, Universidad Nacional del Litoral Santa Fe, ARGENTINA

Contents of this file

Text S1 to S3
Figures S1 to S6

Additional Supporting Information (Files uploaded separately)

Captions for Tables S1 to S7

Introduction

This supplementary text includes extended methods sections for sample preparation and analytical analysis (Text S1), lateral migration rate calculations (Text S2 and Fig. S2) and POC flux calculations (Text S3 and Figs. S2-S5). Supplementary Tables S1-S7 contain all the data used in this manuscript and figures. Table S2 includes data that was originally published in Scheingross et al. (*2021*).

Text S1 - Sample preparation and analytical analysis

We measured suspended sediment grain size distributions by placing sample aliquots (~0.2 g) in plastic test tubes filled with 2.5 ml of dispersion agent (35.68 g Tetrasodium pyrophosphate >99% mixed with 1 L ultra-pure (18.2 MΩ) water) to remove aggregates. Samples were mixed in a rotator for 12-24 h and measured via laser diffraction particle size analysis (Retsch/Horiba LA-950V2). We report particle size distributions based on the median of 10 replicate measurements.

Geochemical analyses (TN, TOC, $\delta^{13}C_{OC}$, and Fm) required ~0.5 g of sample. For samples that had <0.8 g total, we combined two or more consecutive samples to create a new bulk sample with >0.8 g sample mass (Table S1) to performance of both geochemical and grain size analyses. Aliquots for TOC and $\delta^{13}C_{OC}$ measurements were decarbonated prior to analysis following the steps described in Galy et al. (*2007*). Briefly, ~0.5 g of sample are suspended in 7 mL of 4% HCl, vortex mixed, decarbonated in a 80°C water bath for one hour, and frequently vortex mixed during that time. Sample are then centrifuged, the acid is subsequently decanted and samples are washed with ultra-pure (18.2 MΩ) water until they reach a neural pH and are then oven-dried for >48 h at 50°C. TOC, TN, and $\delta^{13}C_{OC}$ measurements were split between facilities at the German Research Centre for Geosciences (GFZ), Durham University, and University of Nevada Reno (UNR). At GFZ and Durham, TOC and $\delta^{13}C_{OC}$ measurements were made using an elemental analyzer (EA, NC2500 Carlo Erba) coupled with a ConFlowIII interface on a DELTAplusXL isotope ratio mass spectrometer (IRMS, ThermoFischer Scientific), and a Costech EA (ECS 4010) connected to a Thermo Finnigan DELTA V Advantage IRMS, respectively. All isotopic compositions are reported using standard delta (δ) notation in per mil (‰) relative to Vienna PeeDee Belemnite (VPDB). Calibration and accuracy were monitored though analyses of in-house standards (Glutamic Acid, 40.82% C, 9.52% N at Durham; Boden3, HEKATECH at GFZ), which were calibrated against international standards (e.g., USGS 40, USGS 24, IAEA 600, IAEA CH3, IAEA CH7, IAEA N1, IAEA N2): this provided a total linear range in $\delta^{13}C_{OC}$ between -46‰ and +3‰. The reproducibility for replicate analyses is 0.2% for TOC and 0.2‰ for $\delta^{13}C_{OC}$ at both institutions. Analytical uncertainty in $\delta^{13}C_{OC}$ was typically <0.1‰ or better for replicate analyses of the international standards.

At UNR, TN was determined using a Euro EA 3000 (Eurovector S.P.A., Milan, Italy). CO_2 production was relatively small, and we achieved good chromatographic separation of N2 vs. CO_2. All Thermal Conductivity Detector (TCD) analyses were calibrated using an acetanilide standard (10.36 wt% N). Linear best-fit line between TCD peak area vs. weight N had a value of R^2 of 0.9995.

Radiocarbon analysis was performed on a selection of suspended sediment, floodplain and soil samples at ETH Zürich. Samples were wrapped in 5x12 mm tin capsules, folded, and analyzed using a combined EA and accelerator mass spectrometer (EA-AMS) (Ruff et al. 2010). The instrumental set-up, blank assessment, accuracy, and reproducibility for the data presented here have been previously reported (*McIntyre et al. 2017*). All $^{14}C/^{12}C$ ratios are reported as fraction modern (Fm, equivalent to $F^{14}C$ as defined by *Reimer et al. (2004)*) relative to 95% of the ^{14}C activity of NBS Oxalic Acid II in 1950 ($\delta^{13}C_{OC}$ = -17.8‰) and normalized to $\delta^{13}C_{OC}$ = -25‰ of VPDB.

Text S2 - Lateral migration rate calculations

Using Sentinel-2 and Planet satellite images (10 m and 3 m resolution, respectively), we delineated the channel at three time-steps with approximately equal temporal spacing to capture one wet and two dry seasons (Fig. 2a). Sentinel-2 images from November 2016 and December 2017 contained clouds that covered up to 25 km of the active river channel, limiting our ability to map the channel extent. For these cases, we used Planet satellite images from within two days of the Sentinel-2 image to supplement the cloud-obscured portion of the Sentinel image. We mapped the channel extent as the wetted area between the two water-bank boundaries, using images when flow was high enough to cover the active channel. We estimate an error of ~2 pixels (~20 m, ~5-13% of the 150-400 m wide channel) on our measured bank position. For each image, we generated a centerline between both channel banks and measured the length of the channel centerline to estimate total channel length. We then converted the two separate channel bank polylines into a binary grid where we assigned areas between the channel banks (i.e., the active river at the time of mapping) a value of 1 and all other areas (i.e., the surrounding floodplain) a value of 0. We estimate the total eroded area during channel migration by subtracting the binary grid for the older time period from the grid for the more recent time period. This allowed us to create a new grid where values of 1 indicate floodplain erosion, values of 0 indicate no change between images, and values of -1 indicate deposition (Fig. S1). For cases where the channel eroded by less than one channel width, the total eroded area can be calculated by summing the pixels with values of 1 and multiplying by the pixel area of ~9 and ~100 m^2, for Planet and Sentinel images, respectively. In one case between December 2016 and June 2017, the channel migrated by more than one channel width. For this case, we analyzed additional images to confirm the channel eroded the entire area between the positions recorded in the December 2016 and June 2017 images, and manually added this area of erosion to *A* in Eq. (1).

We calculated a characteristic sediment transport length, X_{tran}, which represents the average channel length over which the fluvial sediment load exchanges with the floodplain (*Torres et al., 2017*),

$$X_{tran} = \left(\frac{Q_s}{h \times E_{lat}}\right) \quad \text{(S1)}$$

where Q_s is the volumetric river sediment flux, and *h* is the mean channel depth which we set to 5 m (*Repasch et al., 2020*). For the 2017 wet season, X_{tran} = 140 km which corresponds to the distance over which we mapped the channel migration.

Text S3 - OC flux calculation

We calculated the OC flux (Q_{OC}) for our two-year study period by combining rating curves of TOC weight percent and sediment flux as a function of discharge. We first created a TOC-water discharge (Q_w) rating curve by fitting a power law between our measurements of TOC and Q_w (Fig. S4, Table S5):

$$TOC = 1.37 \times Qw^{-0.21} \quad \text{(S2)}$$

Second, we estimated sediment flux using a rate curve based on existing data collected at the El Colorado gauging station (river km 1086) from 2000 to 2017 (Fig. S5 and Table S6, SNIH, https://snih.hidricosargentina.gob.ar/). Suspended sediment fluxes were measured

at approximately monthly intervals, but less frequently during the dry season (June – November) (n = 178). Original sediment flux data were reported for sand (>63 μm) and silt and clay (<63 μm). We use the silt and clay flux to calculate Q_s, because POC in the Río Bermejo is most abundant in fine sediments (*Scheingross et al., 2021*), and our sampling technique captured only silt and clay sized sediment. We calculated a water discharge-sediment flux rating curve using the best-fit power function (Fig. S5) to yield:

$$Q_S = 0.0104 \times Q_w^{1.92} \quad \text{(S3)}$$

We use Eq. S2 to estimate the TOC values over the total discharge record (1992-2018), and calculate the fluvial OC flux (Q_{OC}, Fig. S3, Table S7) by combining Equations (S2) and (S3)

$$Q_{OC} = TOC \times Q_S = 0.0142 \times Q_w^{1.71} \quad \text{(S4)}$$

To estimate the mean contribution of each endmember to the overall OC flux over our two-year study period, we sorted the daily interpolated TOC values by discharge and multiplied the OC flux for each endmember by the mean value of the posterior distribution from the MixSIAR for each discharge bin. We then sorted these values by time and plotted them in Fig. 4b. We extended these calculations of the bedrock and floodplain endmember over the entire 26-year discharge record following the same calculations to estimate the ratio between the bedrock and floodplain endmember.

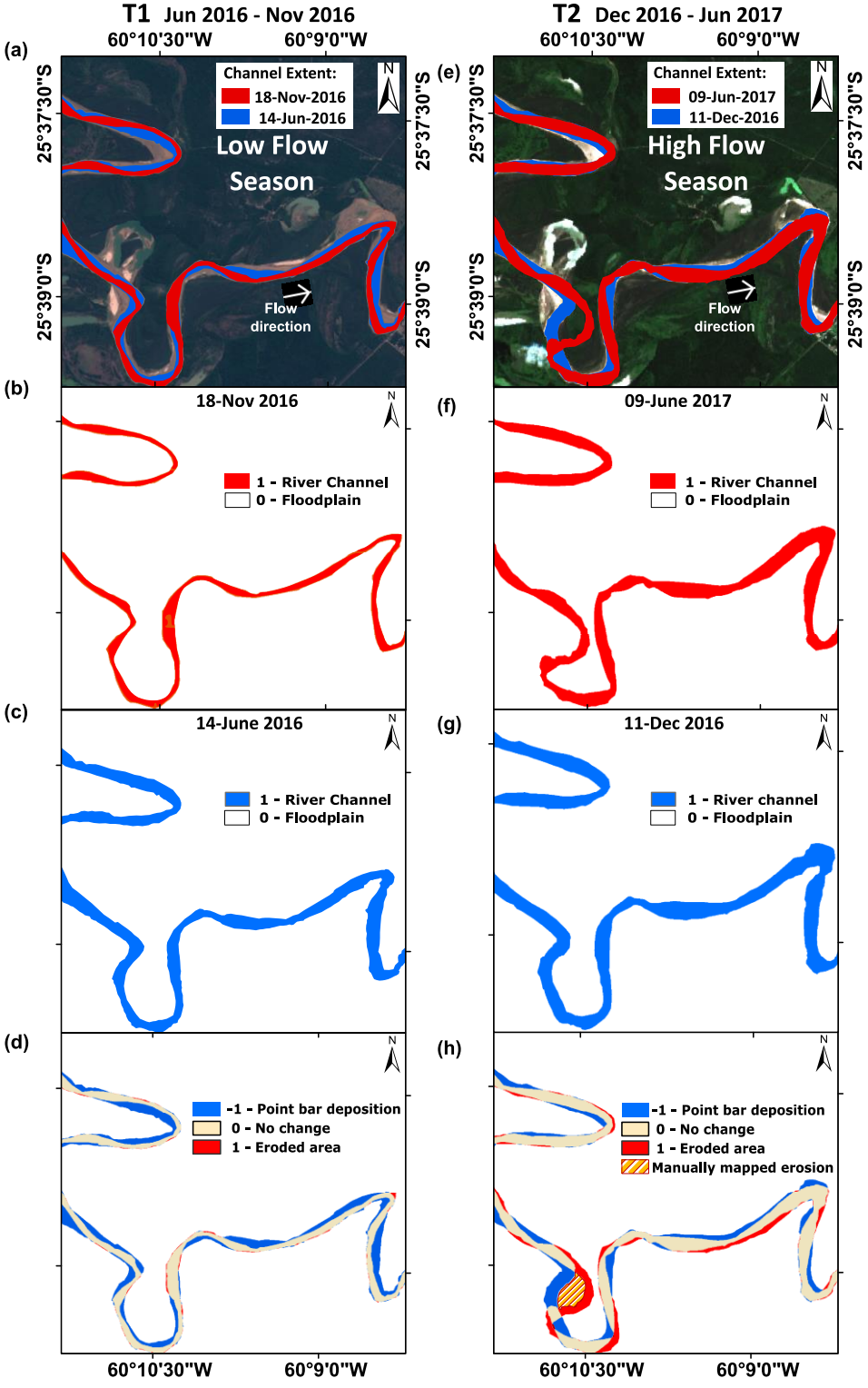

147

148 **Figure S1:** (a-c) and (e-g) Mapped channel extent at the beginning and end of the 2016 dry
149 season (T1) and 2016-2017 wet season (T2), respectively. (d) and (h) Differences between
150 the mapped channel extents at the start and end of T1 and T2, respectively.

151

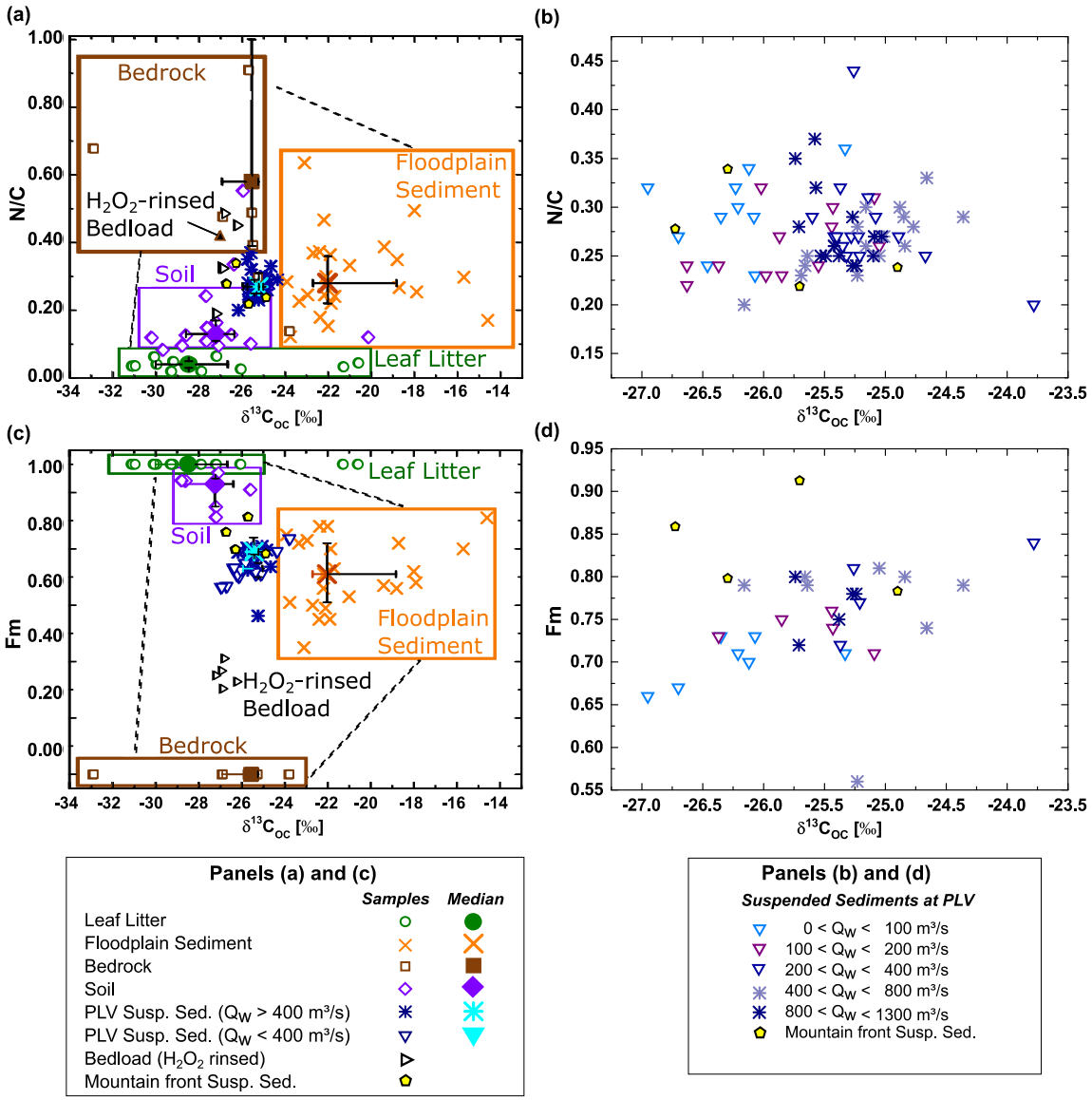

Figure S2: Endmember mixing diagrams showing (a and b) N/C versus $\delta^{13}C_{OC}$, and (c and d) Fm versus $\delta^{13}C_{OC}$. Panels (a) and (c) show PLV suspended sediment, along with soil, leaf litter, floodplain sediment, and bedrock endmembers, where boxes show the range of endmember values. Bedload samples rinsed in H_2O_2 (*Scheingross et al., 2021*) are plotted as black triangles; suspended sediment from the mountain front (the Río Bermejo and Río San Francisco ~10 km upstream of their confluence) is plotted as yellow pentagons. Panels (b) and (d) show a detailed view of PLV suspended sediment data color-coded by the discharge bins used for the MixSIAR analysis.

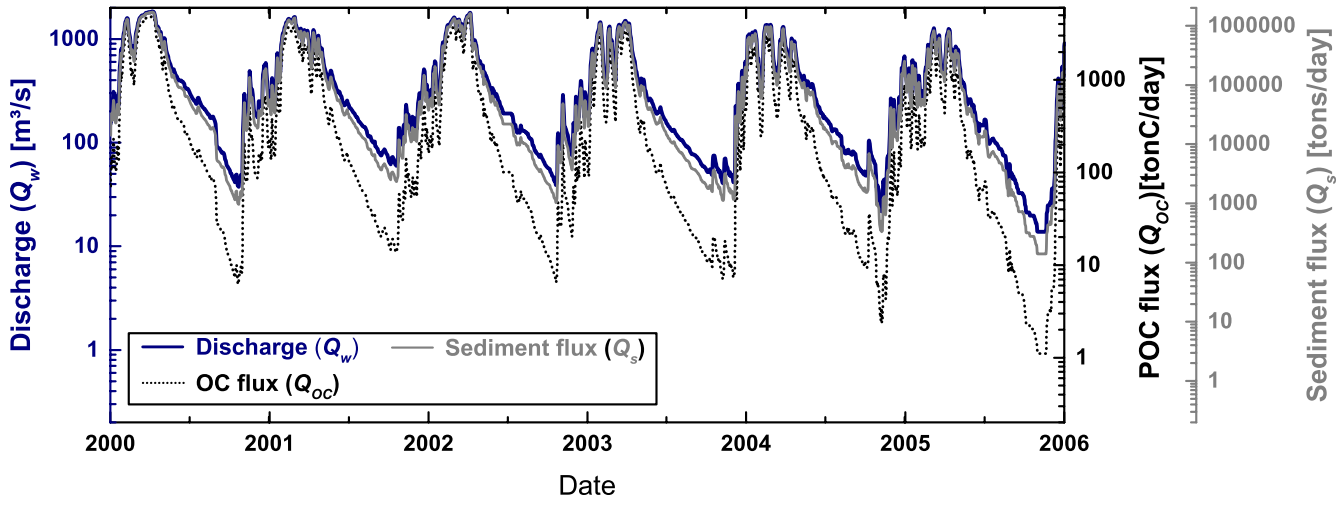

Figure S3: Water, sediment, and POC flux versus time from 2000 – 2006. Trends are similar over the full 26-year time period (1992–2018; Table S7), but we show only 2000-2006 for simplicity.

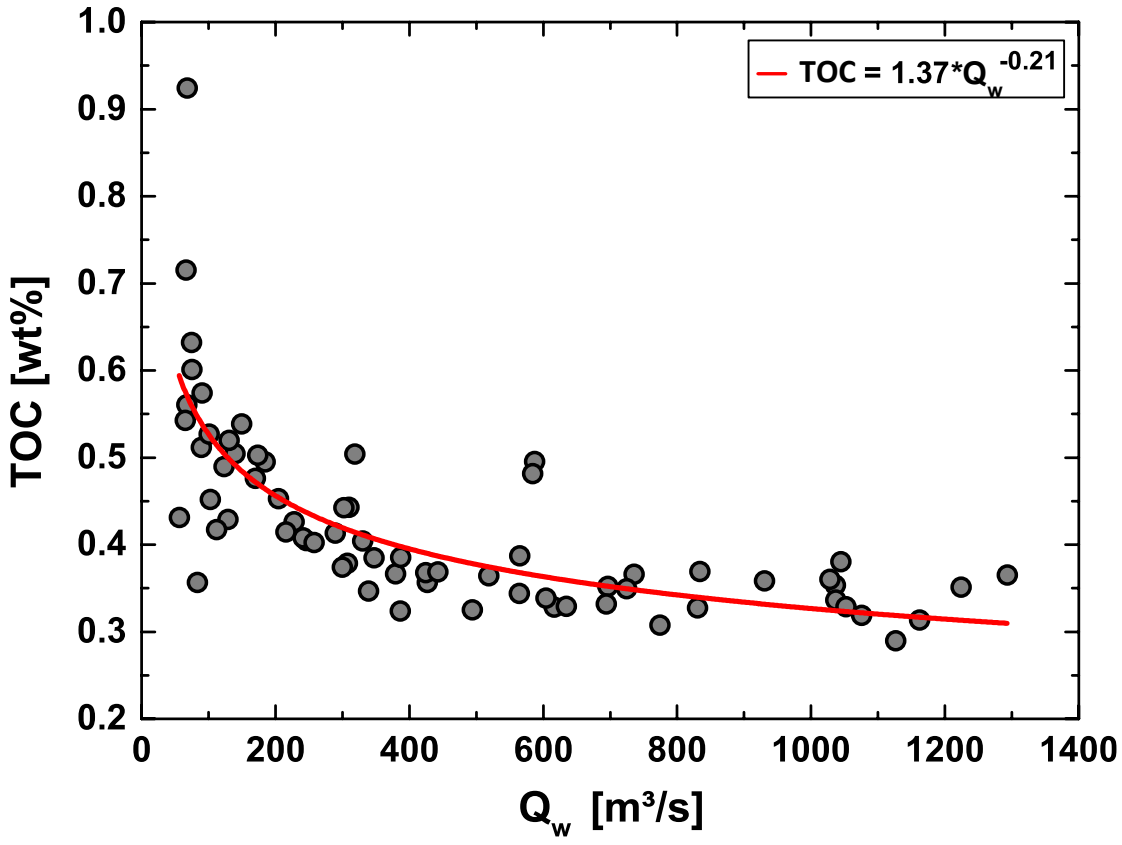

Figure S4: Rating curve for suspended sediment total organic carbon (TOC) weight percent versus water discharge (Q_w) for the data from our two-year study period.

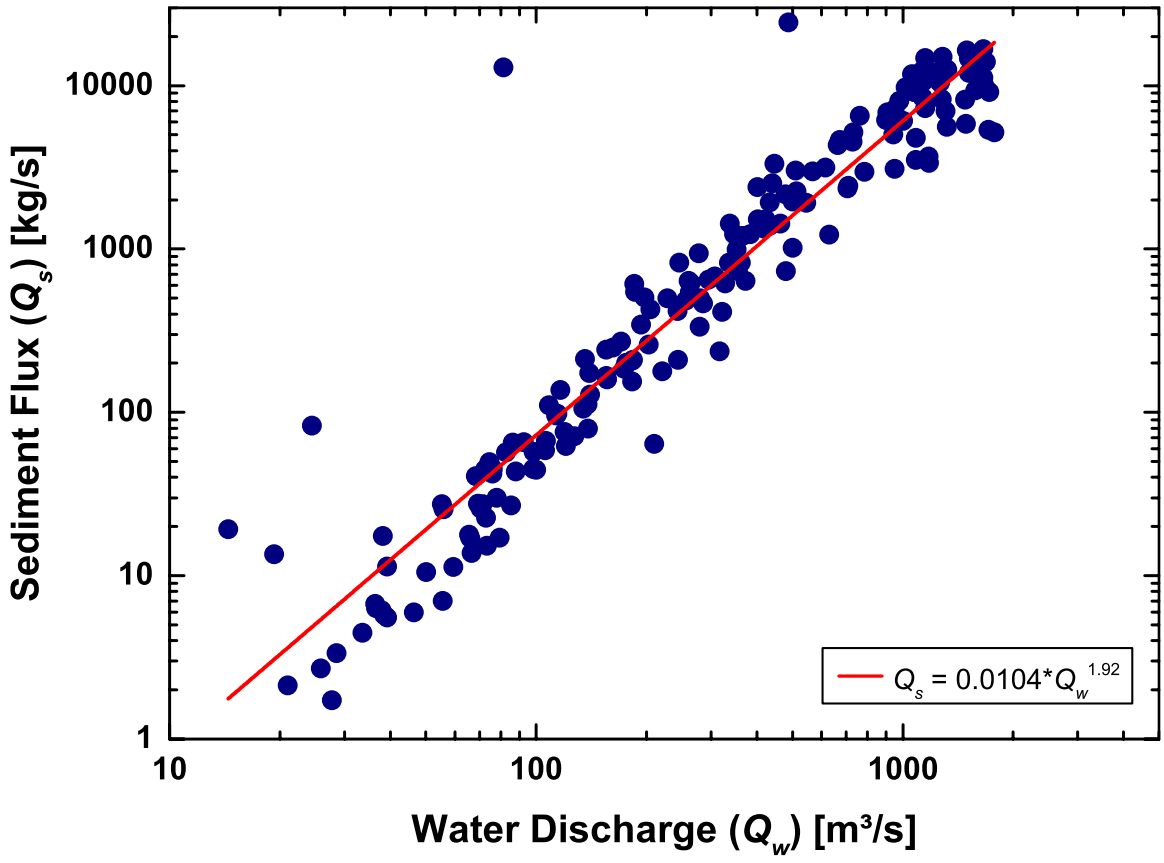

171

172 **Figure S5:** Sediment flux (Q_S) vs. water discharge (Q_W) between 2000 and 2017 at El
173 Colorado station with power-law fit. Q_S is of the combined silt and clay sediment flux
174 reported by SNIH.

175

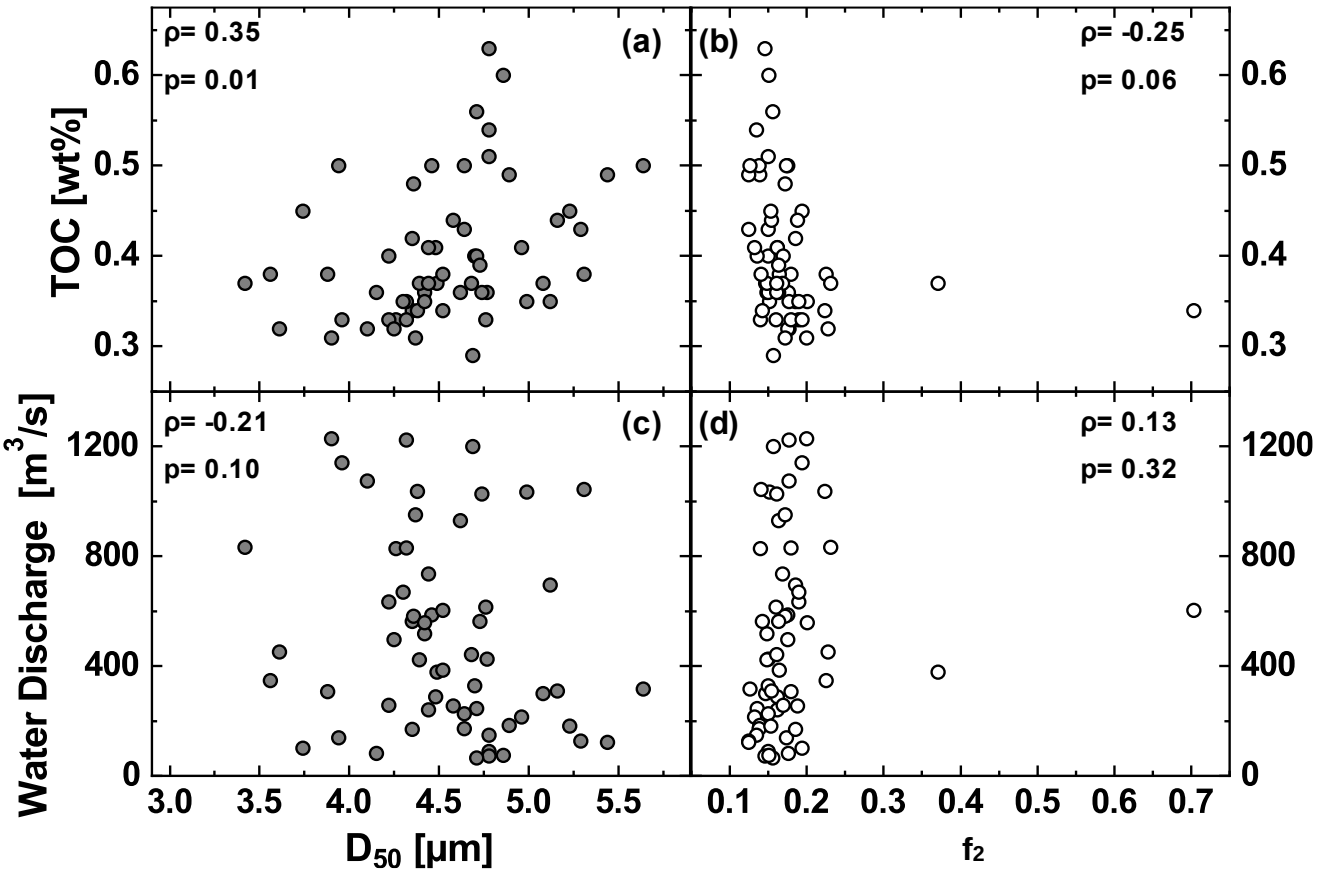

Figure S6: Median grain size and fraction of grains <2µm (f_2) vs. TOC and water discharge. ρ and p are the Pearson correlation coefficient and significance level, respectively.

Table S1. Suspended sediment collected from Puente La Valle (PLV, -25.655º S, -60.130º W) between 2016 – 2018.

Table S2. Overview of endmember samples collected along the Río Bermejo.

Table S3. Endmember data showing TOC-weighted means, standard deviation and standard error.

Table S4. MixSIAR results.

Table S5. Sediment and OC flux calculations for the sampling period between 2016 - 2018.

Table S6. Sediment flux and water discharge data collected between 2000 and 2017 at El Colorado; Source: Sistema Nacional de Información Hídrica (SNIH, https://snih.hidricosargentina.gob.ar/).

Table S7. Water, sediment and POC flux calculations for the full 26-year time period (1992-2018).

References

Sistema Nacional de Información Hídrica (SNIH). Ministerio de Obras Públicas Argentina. Retrieved from https://snih.hidricosargentina.gob.ar/.

Scheingross, J. S., Repasch, M. N., Hovius, N., Sachse, D., Lupker, M., Fuchs, M., et al. (2021). The fate of fluvially-deposited organic carbon during transient floodplain storage. *Earth and Planetary Science Letters, 561*(116822). https://doi.org/10.1016/j.epsl.2021.116822